**Cell Reports, Volume *33***

## Supplemental Information

# Phase-Separated Transcriptional Condensates Accelerate Target-Search Process Revealed by Live-Cell Single-Molecule Imaging

**Samantha Kent, Kyle Brown, Chou-hsun Yang, Njood Alsaihati, Christina Tian, Haobin Wang, and Xiaojun Ren**

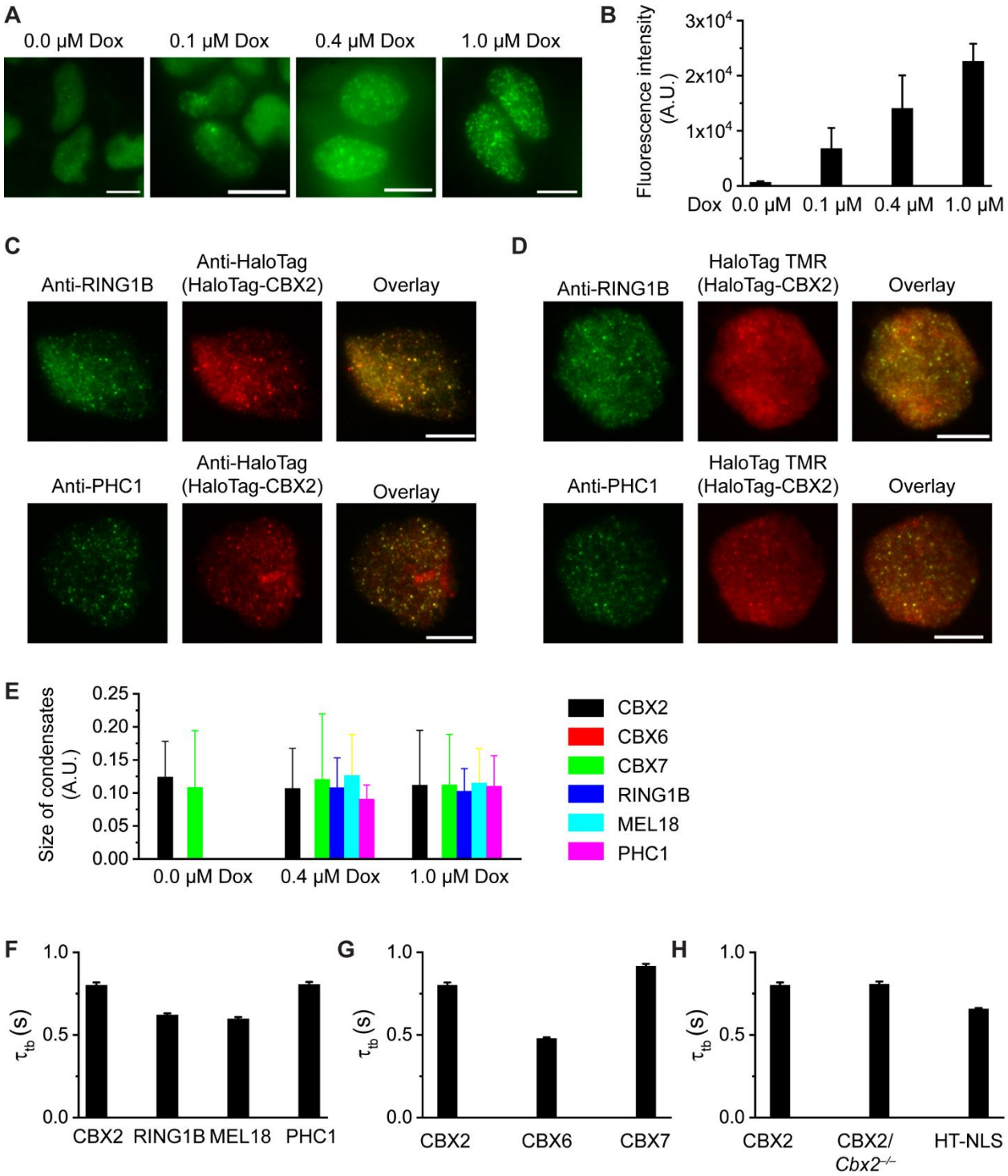


**Figure S1 (related to Figure 1)**. **CBX2 drives the LLPS of CBX-PRC1.**

(**A**) Example live-cell epifluorescence images of HT-CBX2. The expression level of HT-CBX2 was controlled by various doxycycline concentrations indicated above the images. The fusion proteins were labelled with HaloTag TMR ligand. To compare the fluorescence intensities under

different doxycycline concentrations, we took images under the same conditions. Scale bar, 10.0 µm.

(**B**) Fluorescence intensity of HT-CBX2 quantified from Figure S1A. The data were from at least 20 cells per sample. Error bars represent S.D.

(**C**) Example epifluorescence images of co-immunostaining of mESCs expressing HT-CBX2 by using antibodies against RING1B and HaloTag (top panel) or against PHC1 and HaloTag (bottom panel). HT-CBX2 was under the level of basal expression without adding doxycycline. Scale bar, 10.0 µm.

(**D**) Example epifluorescence images of immunostaining of mESCs expressing HT-CBX2 by using antibodies against RING1B (top panel) or PHC1 (bottom panel). HT-CBX2 was induced to express using 1.0 µM doxycycline and labelled with HaloTag TMR ligand. Scale bar, 10.0 µm.

(**E**) Sizes of condensates of HaloTag-PRC1 fusion proteins quantified from Figure 1B. The data were from at least 20 cells per sample. Error bars represent S.D.

(**F-H**) Non-specific residence times ($\tau_{tb}$) quantified from Figure 1E-G. Error bars represent standard error for derived parameter.

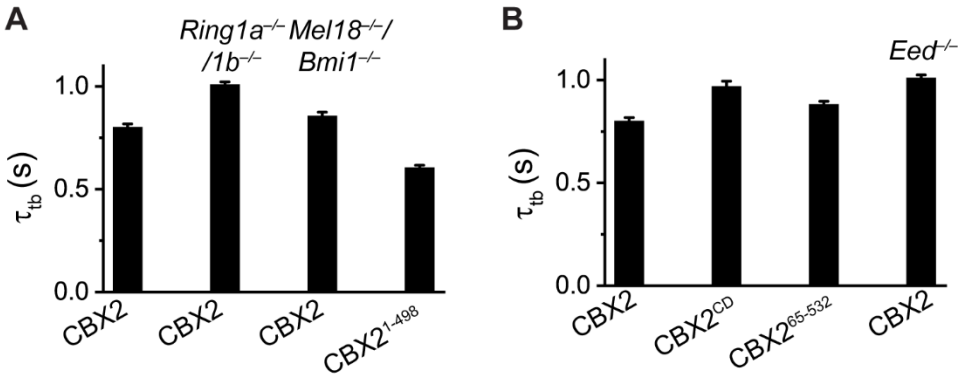


**Figure S2 (related to Figure 2)**. **The binding stability of CBX2 is independent of PRC1 and PRC2.**

(**A**) Non-specific residence times ($\tau_{tb}$) quantified from Figure 2C. Error bars represent standard error for derived parameter.

(**B**) Non-specific residence times ($\tau_{tb}$) quantified from Figure 2F. Error bars represent standard error for derived parameter.

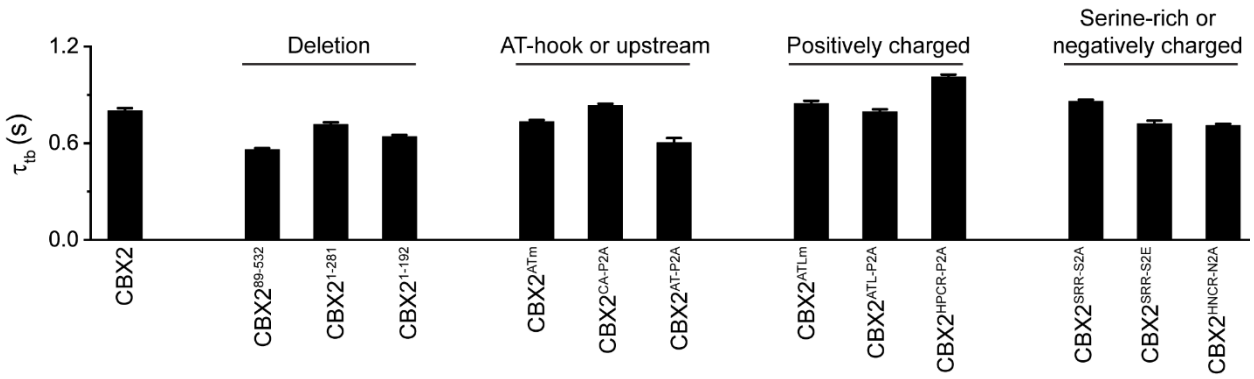


**Figure S3 (related to Figure 3)**. **Effects of mutation and deletion on the condensate formation and binding stability of CBX2.**

Non-specific residence times ($\tau_{tb}$) for CBX2 and its variants quantified from Figure 3B. Error bars represent standard error for derived parameter.

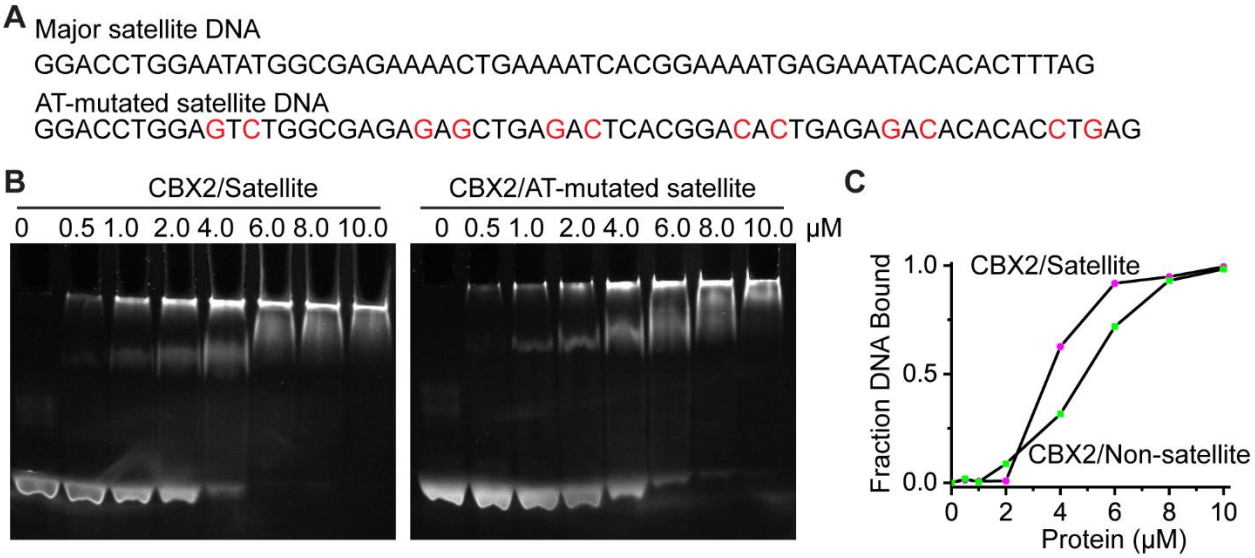


**Figure S4 (related to Figure 4)**. **CBX2 binds DNA, which promotes LLPS *in vitro* and *in vivo*.**

(**A**) Sequences of major satellite DNA and AT-mutated satellite DNA used in the study. The bases highlighted by red are mutations. Sequences are the same length.

(**B**) EMSA determination of CBX2 binding to major satellite DNA and AT-mutated satellite DNA. CBX2 fusion protein concentration is indicated above image.

(**C**) Quantification of EMSA gel in Figure S4B to estimate the dissociation constants of CBX2 to major satellite DNA and AT-mutated satellite DNA.

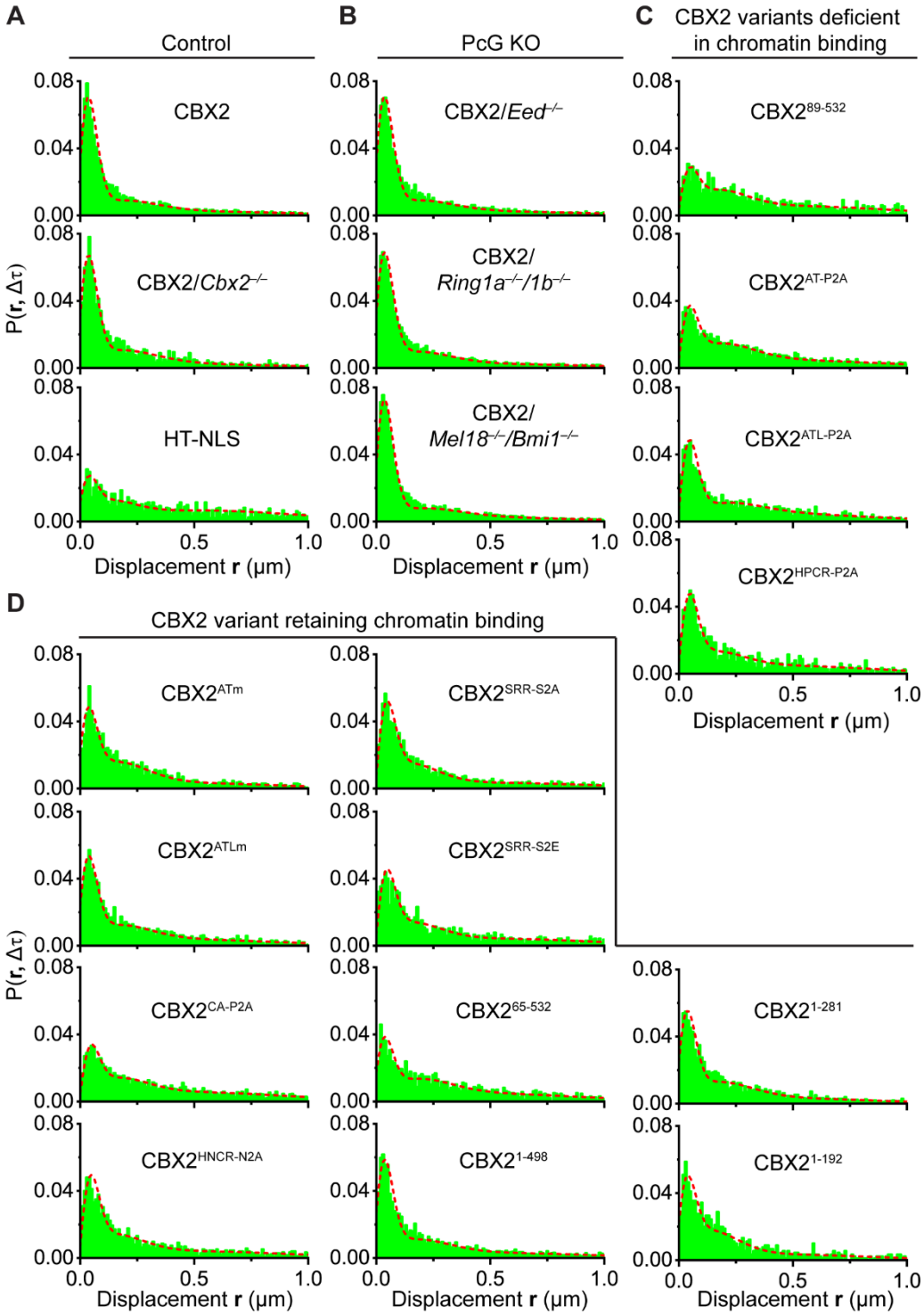


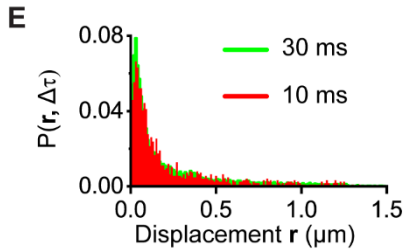


| | $F_1$ (%) | $F_2$ (%) | $F_3$ (%) |
|---|---|---|---|
| 30 ms | 43 ± 4 | 26 ± 4 | 31 ± 3 |
| 10 ms | 40 ± 2 | 24 ± 3 | 36 ± 5 |

**Figure S5 (related to Figure 5)**. **The target-search process of CBX2 and its variants.**

(**A**) Displacement histograms for HT-CBX2 (N = 138 cells, n = 11958 displacements) and HT-NLS (N = 28 cells, n = 2913 displacements) in wild-type mESCs, respectively, and for HT-CBX2 (N = 60 cells, n = 4860 displacements) in *Cbx2*$^{-/-}$ mESCs.

(**B**) Displacement histograms for HT-CBX2 in *Eed*$^{-/-}$ mESCs (N = 65 cells, n = 5802 displacements), *Ring1a*$^{-/-}$/*Ring1b*$^{-/-}$ mESCs (N = 66 cells, n = 9954 displacements) and *Mel18*$^{-/-}$/*Bmi1*$^{-/-}$ mESCs (N = 75 cells, n = 9460 displacements), respectively.

(**C**) Displacement histograms for HT-CBX2$^{89\text{-}532}$ (N = 59 cells, n = 1756 displacements), HT-CBX2$^{AT\text{-}P2A}$ (N = 73 cells, n = 6007 displacements), HT-CBX2$^{ATL\text{-}P2A}$ (N = 62 cells, n = 3662 displacements) and HT-CBX2$^{HPCR\text{-}P2A}$ (N = 68 cells, n = 1474 displacements) in wild-type mESCs, respectively.

(**D**) Displacement histograms for HT-CBX2$^{ATm}$ (N = 77 cells, n = 2557 displacements), HT-CBX2$^{ATLm}$ (N = 77 cells, n = 3579 displacements), HT-CBX2$^{CA\text{-}P2A}$ (N = 68 cells, n = 5013 displacements), HT-CBX2$^{HNCR\text{-}N2A}$ (N = 80 cells, n = 2200 displacements), HT-CBX2$^{SSR\text{-}S2A}$ (N = 134 cells, n = 4120 displacements), HT-CBX2$^{SSR\text{-}S2E}$ (N = 101 cells, n = 2137 displacements), HT-CBX2$^{65\text{-}532}$ (N = 51 cells, n = 2445 displacements), HT-CBX2$^{1\text{-}498}$ (N = 55 cells, n = 5241 displacements), HT-CBX2$^{1\text{-}281}$ (N = 45 cells, n = 3541 displacements) and HT-CBX2$^{1\text{-}192}$ (N = 31 cells, n = 1133 displacements) in wild-type mESCs, respectively.

(**E**) Displacement histograms for HT-CBX2 at 30-ms exposure time with zero dark time (green color) and 10-ms exposure time with 20-ms dark time (red color). Table shows the kinetic fraction of CBX2 at 30-ms exposure time with zero dark time and 10-ms exposure time with 20-ms dark time.

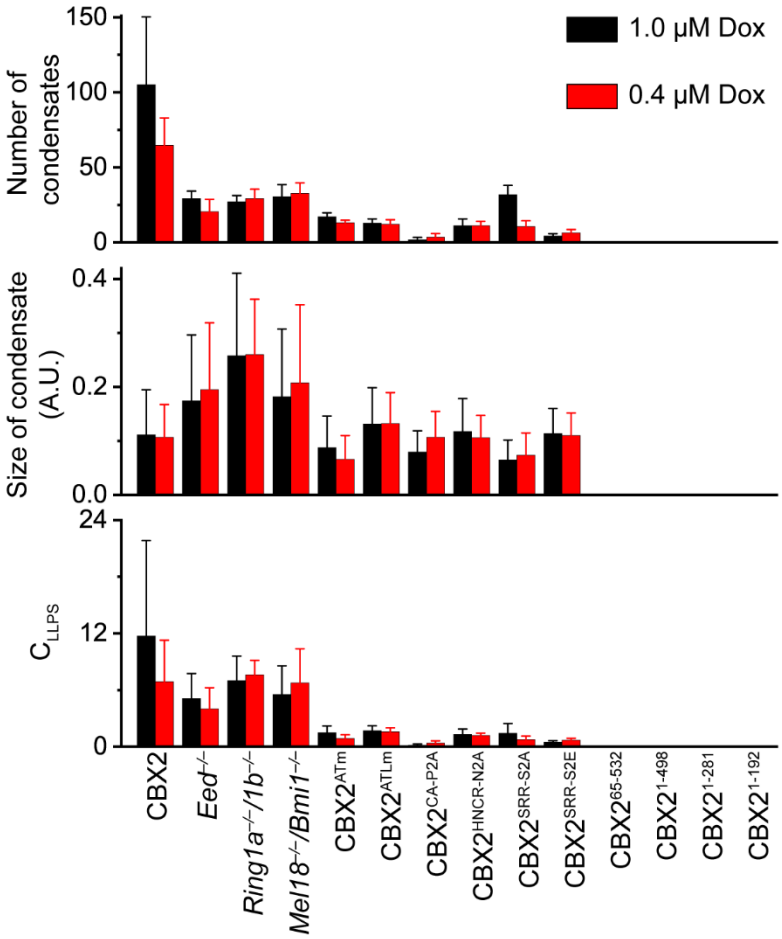


**Figure S6 (related to Figure 6)**. **LLPS speeds up the target-search process of CBX2.** Number, size and $C_{LLPS}$ for CBX2 and its variants under 0.4 and 1.0 μM doxycycline. A.U., arbitrary unit. Error bars represent S.D.

**Table S1. Number of cells and trajectories/displacements used in Figures.**

| | | Protein/cell | Number of cells | Number of trajectories/displacements |
|---|---|---|---|---|
| Figure 1 | Figure 1E | HT-CBX2/wt | 45 | 5104 |
| | | HT-RING1B/wt | 82 | 1990 |
| | | HT-MEL18/wt | 53 | 1785 |
| | | HT-PHC1/wt | 126 | 3230 |
| | Figure 1F | HT-CBX2/wt | 45 | 5104 |
| | | HT-CBX6/wt | 29 | 949 |
| | | HT-CBX7/wt | 42 | 4076 |
| | Figure 1G | HT-CBX2/wt | 45 | 5104 |
| | | HT-CBX2/*Cbx2*$^{-/-}$ | 20 | 1681 |
| | | HT-NLS/wt | 43 | 1991 |
| Figure 2 | Figure 2C | HT-CBX2/wt | 45 | 5104 |
| | | HT-CBX2/ *Ring1a*$^{-/-}$/*Ring1b*$^{-/-}$ | 29 | 2616 |
| | | HT-CBX2/ *Mel18*$^{-/-}$/*Bmi1*$^{-/-}$ | 21 | 1849 |
| | | HT-CBX2$^{1\text{-}498}$/wt | 42 | 2244 |
| | Figure 2F | HT-CBX2/wt | 45 | 5104 |
| | | HT-CBX2$^{CD}$/wt | 58 | 3152 |
| | | HT-CBX2$^{65\text{-}532}$/wt | 52 | 1154 |
| | | HT-CBX2/*Eed*$^{-/-}$ | 36 | 1838 |
| Figure 3 | Figure 3B | HT-CBX2/wt | 45 | 5104 |
| | | HT-CBX2$^{89\text{-}532}$/wt | 42 | 1364 |
| | | HT-CBX2$^{1\text{-}281}$/wt | 32 | 1478 |
| | | HT-CBX2$^{1\text{-}192}$/wt | 47 | 1336 |
| | | HT-CBX2$^{ATm}$/wt | 53 | 1994 |
| | | HT-CBX2$^{CA\text{-}P2A}$/wt | 42 | 1176 |
| | | HT-CBX2$^{AT\text{-}P2A}$/wt | 43 | 1121 |
| | | HT-CBX2$^{ATLm}$/wt | 49 | 2972 |
| | | HT-CBX2$^{ATL\text{-}P2A}$/wt | 40 | 2648 |
| | | HT-CBX2$^{HPCR\text{-}P2A}$/wt | 48 | 3084 |
| | | HT-CBX2$^{SRR\text{-}S2A}$/wt | 134 | 4102 |
| | | HT-CBX2$^{SRR\text{-}S2E}$/wt | 101 | 2137 |
| | | HT-CBX2$^{HNCR\text{-}N2A}$/wt | 80 | 2200 |
| | | HT-CBX2/wt | 138 | 11958 |
| | | HT-CBX2/*Cbx2*$^{-/-}$ | 28 | 2913 |
| | | HT-NLS/wt | 60 | 4860 |
| | | HT-CBX2/*Eed*$^{-/-}$ | 65 | 5802 |
| | | HT-CBX2/ *Ring1a*$^{-/-}$/*Ring1b*$^{-/-}$ | 66 | 9954 |

| | | | | |
|---|---|---|---|---|
| Figure 5 | Figure 5B-E | HT-CBX2/ *Mel18*$^{-/-}$/*Bmi1*$^{-/-}$ | 75 | 9460 |
| | | HT-CBX2$^{89\text{-}532}$/wt | 59 | 1756 |
| | | HT-CBX2$^{AT\text{-}P2A}$/wt | 73 | 6007 |
| | | HT-CBX2$^{ATL\text{-}P2A}$/wt | 62 | 3662 |
| | | HT-CBX2$^{HPCR\text{-}P2A}$/wt | 68 | 1474 |
| | | HT-CBX2$^{ATm}$/wt | 77 | 2557 |
| | | HT-CBX2$^{ATLm}$/wt | 77 | 3579 |
| | | HT-CBX2$^{CA\text{-}P2A}$/wt | 68 | 5013 |
| | | HT-CBX2$^{HNCR\text{-}N2A}$/wt | 80 | 2200 |
| | | HT-CBX2$^{SRR\text{-}S2A}$/wt | 134 | 4120 |
| | | HT-CBX2$^{SRR\text{-}S2E}$/wt | 101 | 2137 |
| | | HT-CBX2$^{65\text{-}532}$/wt | 51 | 2445 |
| | | HT-CBX2$^{1\text{-}498}$/wt | 55 | 5241 |
| | | HT-CBX2$^{1\text{-}281}$/wt | 45 | 3541 |
| | | HT-CBX2$^{1\text{-}192}$/wt | 31 | 1133 |

The wt denotes wild-type mESCs. Others are knockout mESCs.